Immunohistochemical detection of double-stranded RNA in formalin-fixed paraffin-embedded tissue

Thomsen, Christian; Røge, Rasmus; Fred, Åsa; Wanders, Alkwin

Published in:
APMIS

DOI (link to publication from Publisher):
10.1111/apm.13300

Publication date:
2023

Document Version
Publisher's PDF, also known as Version of record

APMIS JOURNAL OF PATHOLOGY, MICROBIOLOGY AND IMMUNOLOGY

APMIS 131: 197–205 © *2023 The Authors. APMIS* published by John Wiley & Sons Ltd on behalf of Scandinavian Societies for Pathology, Medical Microbiology and Immunology.

DOI 10.1111/apm.13300

Immunohistochemical detection of double-stranded RNA in formalin-fixed paraffin-embedded tissue

CHRISTIAN THOMSEN,[1,2] RASMUS RØGE,[1,2] ÅSA FRED[3,4] and ALKWIN WANDERS[1,2]

[1]Department of Pathology, Aalborg University Hospital; [2]Department of Clinical Medicine, Aalborg University, Aalborg, Denmark; [3]Department of Pathology, Halmstad Hospital, Halmstad; and [4]Department of Pathology, Sahlgrenska University Hospital, Gothenburg, Sweden

Thomsen C, Røge R, saFred, Wanders A. Immunohistochemical detection of double-stranded RNA in formalin-fixed paraffin-embedded tissue. APMIS. 2023; 131: 197–205.

Double-stranded RNA (dsRNA) is produced during most viral infections, and immunohistochemical detection of dsRNA has been proposed as a potential screening marker for viral replication. The anti-dsRNA monoclonal antibody clone 9D5 is more sensitive than the established clone J2 but has not been validated in formalin-fixed paraffin-embedded (FFPE) tissue. This study aimed to test and compare the performance of the anti-dsRNA monoclonal antibodies, 9D5 and J2, in FFPE tissue using an automated staining platform. Archived clinical tissue samples with viral infections (n = 34) and uninfected controls (n = 30) were examined. Immunohistochemical staining for dsRNA (9D5 and J2) and virus-specific epitopes was performed. 9D5 provided a similar staining pattern but a higher signal-to-noise ratio than J2. The following proportions of virus-infected tissue samples were dsRNA-positive: SARS-CoV-2 (5/5), HPV (6/6), MCV (5/5), CMV (5/6), HSV (4/6), and EBV (0/6). Also, 18 of 30 uninfected samples were dsRNA positive, and an association between fixation time and intensity was observed. However, signals in all samples were markedly reduced by pretreatment with dsRNA-specific RNAse-III, indicating a specific reaction. In conclusion, dsRNA can be demonstrated in most viral infections with immunohistochemistry in FFPE tissue but with low clinical specificity. The antibody clone 9D5 performs better than clone J2.

Key words: Double-stranded RNA; FFPE; formalin; immunohistochemistry; virus.

Christian Thomsen, Department of Pathology, Aalborg University Hospital, Ladegaardsgade 3, Aalborg DK-9000, Denmark. e-mail: christian.t@rn.dk

Demonstrating viral infection in tissue specimens may benefit several situations, even without knowing the specific virus type. With new viruses, such as SARS-CoV-2, early detection may be valuable before more specific methods are developed and may play a role in validating such methods [1]. Another situation is screening for viral infection in clinical samples, in cases with certain cytological or histological changes where viral infections are among the differential diagnoses. Simple exclusion or demonstration of viral infection would enable the pathologist to make a more concise diagnosis in such cases.

Another application is in the study of chronic disorders where persistent viral infections have been suggested to play an important role, such as diabetes and Crohn's disease [2,3]. In pathology laboratories, archival materials of tissue specimens with numerous chronic inflammatory diseases are available and may serve as an invaluable source for etiological studies. However, most of these specimens are formalin-fixed and paraffin-embedded (FFPE), which limits the sensitivity of methods based on the detection of nucleic acids, such as *in situ* hybridization, polymerase chain reaction, and next-generation sequencing. Besides that, single-stranded RNA viruses have a relatively high mutation rate making it difficult to design matching probes [4,5]. By contrast, modern immunohistochemistry (IHC) is a method optimized for FFPE tissue. Antibodies against specific viruses exist, but IHC-based screening tools for viral detection are missing.

One way of detecting virus infection is the demonstration of double-stranded RNA (dsRNA) by pattern recognition, as the innate immune system does. Typically, dsRNA molecules of more than ~30 nucleotides in length are not present in the cytosol of human cells but are produced in varying

Received 12 October 2022. Accepted 5 February 2023

amounts during viral replication [6]. Detection of dsRNA in an infected cell by cytosolic pattern recognition receptors, such as the interferon-induced dsRNA-dependent kinase (PKR), leads to the production of type-I interferons and an anti-viral state of the infected cell [7–9]. Small amounts of endogenous dsRNA may exist in the mitochondria and nucleus, where cellular membranes keep it segregated from the pattern recognition receptors in the cytosol [10].

Monoclonal anti-dsRNA antibodies (Abs) have been proposed as a screening tool for viral infections and have also been used to detect endogenous dsRNA [6,11,12]. A few anti-dsRNA Abs are commercially available that bind sequence-non-specific dsRNA segments longer than ~40 nucleotides [13]. Only two of these Ab clones, J2 and K1, have been reported to function in FFPE tissue samples [11]. J2 and K1 have very comparable characteristics. J2 has been investigated more thoroughly than K1 and proven unable to detect negative-sense single-stranded RNA viruses [14,15]. On the other hand, this can be accomplished by another Ab clone, 9D5, but it has never been described in FFPE tissue samples [6,16].

This study aimed to test and compare the performance of the anti-dsRNA monoclonal antibodies J2 and 9D5 in virus-infected and normal FFPE specimens.

MATERIALS AND METHODS

Tissues

Formalin-fixed paraffin-embedded-tissue samples with reported (morphologically and/or immunohistochemically) viral infection were identified at the Department of Pathology, Aalborg University Hospital, Denmark, using the local database system. Tissues with the following viral infections were obtained: SARS-CoV-2, herpes simplex virus (HSV), cytomegalovirus (CMV), human papillomavirus (HPV), molluscum contagiosum virus (MCV), and Epstein–Barr virus (EBV). SARS-CoV-2 has a positive-sense single-stranded RNA (+ssRNA) genome, while the remaining viruses have a dsDNA genome. Many samples were available for HPV, HSV, MCV, and EBV, and five tissues with each virus were selected. All available cases from 2010–2022 were included for the remaining viruses. Tissues used in routine diagnostics as on-slide controls for the abovementioned viruses (except MCV) were also included. In addition, autopsy material from the lungs of one patient with SARS-CoV-2 infection was received from the Department of Pathology, Halmstad Hospital, Sweden.

Histomorphological non-neoplastic and non-infected tissues from the same topographic sites were included as controls, with five samples from different patients from each site (central nervous system, tonsil, lung, lymph node, skin, placenta). These tissues were regarded as 'uninfected'.

All tissue samples had been fixed for at least 24 h in 10% neutral-buffered formalin. All materials were anonymized immediately after inclusion in the study.

Tissue microarrays

Three tissue microarrays (TMA) were constructed from the included material using a TMA Grand Master (3D Histotech, Budapest, Hungary; core diameter: 2 mm). Two TMAs contained 18 cores with virus-infected tissues, while the last TMA contained 30 cores with uninfected tissues. Eight samples with HSV (n = 4) and MCV (n = 4) were too small for inclusion in the TMAs and were studied as whole sections. Two additional TMAs (from a previous fixation project) were included, containing tonsillar and colorectal tissue from two individual patients, which had been fixed for 3, 24, 48, and 168 h.

Immunohistochemistry

3 μm sections were cut from each TMA/tissue block and mounted on coated slides (Dako FLEX IHC slides K8020, Agilent, Glostrup, Denmark). The sections were dried for 2 days at room temperature and then stored at −20 °C until staining. The slides were baked at 60 °C for at least 30 min and then placed in the automated Ventana BenchMark Ultra instrument (Roche Diagnostics, Copenhagen, Denmark), except for HSV (Dako Omnis instrument, Agilent). Protocol details are listed in Table 1. In general, slides were deparaffinized on board and submitted to heat-induced epitope retrieval (HIER) in buffer at 99 °C. Following endogenous peroxidase blocking, the primary Abs (see Table 1) were applied for 32 min at 36 °C. After a wash in buffer, the visualization system was applied, and the slides were finally developed with chromogen and counterstained with hematoxylin II (Ventana 790–2208, Roche Diagnostics).

The protocol settings for 9D5 and J2 were determined following a comprehensive optimization procedure, using SARS-CoV-2-infected tissue as positive control and a TMA with 20 different uninfected tissues (some of which were negative) as reference. The staining protocols for each dsRNA antibody clone were optimized in the following way, aiming for the highest possible signal-to-noise ratio: Different dilutions were tested (J2 range: 1:500–1:4000, 9D5 range: 1:1000–1:64 000) using our in-house standard protocol (HIER: pH 9.0 for 48 min. at 99 °C) to find a possible range of optimal concentrations. Subsequently, pH 6.0 for 48 min was used for both clones. The buffer gaining the best results was combined with proteinase K (HIER 16 min + proteinase 4 min.) or proteinase K alone for 8 min. Finally, the dilutions were optimized once more. The resulting protocols were: J2 1:3000, pH 6.0 at 99 °C for 48 min; 9D5 1:16 000, pH 9.0 at 99 °C for 48 min. Two pathologists judged all stained slides from the optimization procedure. The dsRNA Abs were tested on the automated Dako Omnis Instrument without satisfying results.

Pretreatment by RNAse-III (degrades dsRNA) to test specificity

The IHC protocol was stopped after pretreatment/epitope retrieval, and a hydrophobic barrier was drawn on the

Table 1. Immunohistochemistry and ISH

Target	Antibody clone	Type	Vendor	Product no.	HIER time (min), buffer	Dilution[1]	Visualization
dsRNA	J2	Mouse monoclonal	Scicons, Budapest, HUN	10010500	48, CC2	1:3000	Optiview DAB
dsRNA	9D5	Mouse monoclonal	Absolute antibody, Redcar, UK	Ab00458-1.1	48, CC1	1:16 000	Optiview DAB
SARS	-	Rabbit polyclonal	Novus biologicals, Centennial, CO, USA	NB100-56576	36, CC1	1:2000	Ultraview RED + Amp
CMV	CCH2 + DDG9	Mouse monoclonal	DAKO Agilent, Glostrup, DK	M 085401	48, CC1	1:25	Optiview DAB
HSV[2]	-	Rabbit polyclonal	DAKO Agilent, Glostrup, DK	GA52161	30, TRS low pH	RTU	EnVision Flex
EBER	-	*In situ* hybridization	Roche, Oro Valley, AZ, USA	800–2842	16, CC2 + 4, ISH Proteinase 3	RTU	iview blue ISR
HPV	IH8[3]	Mouse monoclonal	Chemicon, Søborg, DK	MAB837	48, CC1	1:1000	Optiview DAB

Visualization systems: OptiView DAB. HRP-labeled multimer, Ventana, 760–700, Roche, Oro Valley, AZ, USA; Ultraview RED. Ultraview universal alkaline phosphatase red detection kit, Ventana, 760–501, Roche, Oro Valley, AZ, USA; Amp. Optiview amplification kit, Ventana, 760–099, Roche, Oro Valley, AZ, USA; EnVision Flex. Dako, GV800, Agilent, Glostrup, DK; TRS low pH. Envision Flex, Dako GV805, Agilent, Glostrup, DK; ISH iView blue detection kit. Ventana, 800–092, Roche, Oro Valley, AZ, USA.
[1]Dilution buffer: EnVision Flex Antibody Diluent, Dako Agilent, Glostrup, DK.
[2]Dako Omnis instrument.
[3]HPV-1, 6, 11, 16, 18 and 31.

slide. Each slide was then incubated with the following solution (total 200 µL) for 2 h at 37 °C: 140 µL distilled water, 20 µL ShortCut Reaction Buffer (New England Biolabs, Ipswich, MA, USA), 20 µL (40 Units) ShortCut RNase III (New England Biolabs, Ipswich, MA, USA), and 20 µL MnCl2. Finally, 10 µL EDTA was added to stop the reaction, and the IHC protocol was continued. Control slides were treated equally, except for the exclusion of RNase III (20 µL distilled water was added instead).

Interpretation

Three pathologists annotated all sections independently, and the results were discussed together until consensus was obtained. This assessment included technical analysis of the signal-to-noise ratio and a comparison of the staining reaction between the antibodies. Regarding dsRNA, cells containing no or weak signals were classified as negative, whereas moderate or high signal intensity was classified as positive. dsRNA-positive plasma cells and endothelial cells were not included in the annotation because these cells were not considered tissue-specific.

RESULTS

We found that dsRNA could be detected in FFPE-tissue by IHC using an automated staining platform. The antibodies 9D5 and J2 had very similar staining patterns. Despite a more significant antibody dilution (see Table 1), 9D5 generally provided a stronger signal and a higher signal-to-noise ratio than J2. Results are summarized in Table 2.

Examples of dsRNA in virus-infected tissues are displayed in Fig. 1.

dsRNA was demonstrated in lung tissue with SARS-CoV-2 infection by both antibodies, J2 and 9D5. The positive cells were mainly macrophages based on CD68 stained serial sections (data not shown). A similar pattern was seen with the control anti-SARS IHC. Corresponding cells were positive in one of five uninfected samples by J2, whereas all were negative with 9D5. Four cases with SARS-CoV-2-infected placentas were also included. Anti-SARS IHC showed a varying reaction in the trophoblast. Accordingly, the trophoblast was dsRNA-positive in all four cases with 9D5 and three with J2. Stroma cells were positive in two and three cases, respectively. Of the five uninfected placenta samples, all had positive stromal cells with 9D5, and one also had positive trophoblast cells. Only two uninfected samples were positive in the stromal cells with J2.

The material included a single case with HSV encephalitis (brain tissue). dsRNA was demonstrated in neurons by J2 and 9D5, but the number of positive cells was less than observed with anti-HSV IHC. All five samples with uninfected brain

Table 2. Summary of the investigated tissue specimen with the positivity for dsRNA achieved by staining with the antibody clones J2 and 9D5

	Infected (pos/total)[1]		Uninfected (pos/total)	
Tissue type (virus), (n infected; n uninfected)	J2	9D5	J2	9D5
Lung (SARS-CoV2), (1; 5)				
Alveolar lining	1/1	1/1	1/5	0/5
Bronchial epithelium	1/1	0/1	1/3[2]	0/3[2]
Macrophages	1/1	1/1	3/5	0/5
Placenta (SARS-CoV2), (4; 5)				
Trophoblast	3/4	4/4	0/5	1/5
Stroma	3/4	2/4	2/5	5/5
Placenta (CMV), (6; 5)				
Trophoblast	0/6	5/6	"	"
Stroma	2/6	5/6	"	"
Central nervous system (HSV), (1; 5)				
Neurons	1/1	1/1	3/5	5/5
Skin (HSV), (5; 5)				
Squamous epithelium	4/5	3/5	1/5	1/5
Skin (HPV), (6; 5)				
Squamous epithelium	5/6	6/6	"	"
Skin (MCV), (5; 5)				
Squamous epithelium	5/5	5/5	"	"
Tonsil (EBV), (3; 5)				
Squamous epithelium	3/3	2/3	5/5	5/5
Lymphoid tissue	NA[3]	0/3	NA[3]	2/5
Lymph node (EBV), (3; 5)				
Lymphoid tissue	NA[3]	0/3	NA[3]	3/5

[1]Plasma cells and endothelial cells excluded.
[2]Bronchial epithelium was only represented in three of the five uninfected cases.
[3]Not assessable due to high-background staining reaction.

tissue were positive in neurons for dsRNA with 9D5 (see Fig. 2), whereas J2 was positive only in three samples. There was a considerable variation in the ratio and intensity of positive cells between the samples.

In four of the six cases of EBV infection, there was only a weak reaction in the cytoplasm of morphologically infected lymphoid cells with 9D5, thereby not sufficient intensity to be regarded as positive. By contrast, all six cases showed widespread and intense positivity for EBER. The corresponding uninfected tonsils had all positive squamous epithelium, while the lymphoid tissue was positive in two of the five samples (see Fig. 2). Two of five lymph nodes were positive in the germinal centers. In all samples with lymphoid tissue, clone J2 provided too much background to assess if there were any true staining reactions.

Three different skin infections were included. In all six cases of condylomas, a staining reaction was seen in the basal and spinous layers of the squamous epithelium by clone 9D5 (five by J2). All cases were positive when using an HPV IHC assay against six different HPV subtypes. Unlike dsRNA, the reaction was limited to a few cells in the granular layer and stratum corneum. All five cases with MCV infection were strongly positive for dsRNA with both Ab clones in the keratinocytes with viral inclusions. The reaction was most intense in the spinous layer and decreased toward the surface. Of the five HSV-infected cases, dsRNA could be demonstrated in four cases by J2, but only three by 9D5. The reaction was mainly nuclear, corresponding to nuclear viral inclusions of the infected keratinocytes. However, compared with anti-HSV IHC, only a subset of the infected cells were dsRNA positive. Regarding uninfected skin, one of five samples was positive with 9D5 and J2 (see Fig. 2).

Six cases with proven placental CMV infection were evaluated. Anti-CMV IHC was positive in scattered stromal cells, while in five cases, dsRNA was positive in a higher number of cells in both stroma and trophoblast with clone 9D5. J2 was only positive in the stromal cells in two cases.

Irrespective of the tissue type and infectious status, a large proportion of the samples showed strong positivity for dsRNA in plasma cells and endothelial cells.

Preincubation of the tissue with RNase III resulted in most cases in total abrogation of the dsRNA signals (see Fig. 3). In the remaining cases, the signal intensity was significantly reduced. We observed no unaltered signals following RNAse-III treatment.

dsRNA IHC staining of tonsillar and colorectal tissues with different fixation times showed no or

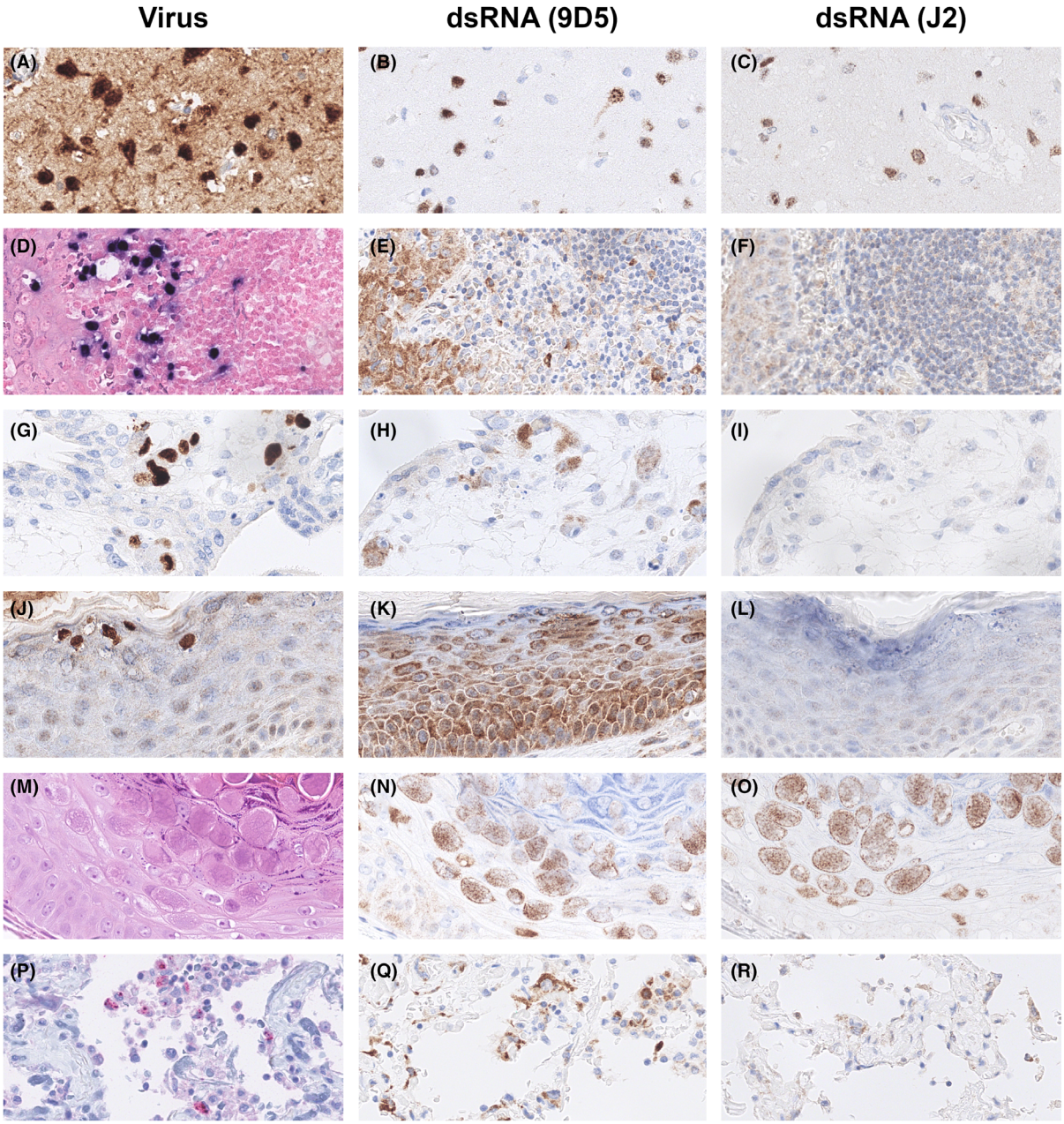

Fig. 1. Immunohistochemical expression of dsRNA in virus-infected tissues. The pictures in the left column show tissues stained with virus-specific markers or hematoxylin–eosin. The pictures in the middle and right columns show immunohistochemical stainings of the same tissues using the anti-dsRNA antibody clones 9D5 and J2, respectively. (A–C), Herpes simplex-infected brain tissue. Intense and widespread reaction with anti-HSV (brown) in neurons. A moderate to strong reaction for dsRNA (brown) with both 9D5 and J2. (D–F), Tonsil infected by Epstein–Barr virus. Intense reaction for EBER ISH (blue) in many lymphoid cells while, in both dsRNA stainings, the corresponding cells display only a weak positivity. Moderate reaction for dsRNA is observed in the squamous epithelium and some other cells of the tonsillar tissue with 9D5. (G–I), Cytomegalovirus infection in placenta. Strong reaction for anti-CMV (brown) in many stromal cells. 9D5 is moderately positive in similar cells and weakly in the trophoblast. J2 is negative. (J–L), Condyloma with human papillomavirus. Anti-HPV (brown) with strong reaction in the superficial layers of the squamous epithelium. 9D5 is moderate to strongly positive in the basal and spinous layers. J2 shows a weak reaction. (M–O), Molluscum contagiosum virus infection in the skin. Conspicuous viral inclusions on HE. Correspondingly moderate to strong reaction with both anti-dsRNA clones. (P–R), Lung with SARS-CoV2. Strong reaction with anti-SARS antibody (red) in some interalveolar cells. Reaction against dsRNA is more intense and includes more cells with 9D5. J2 shows a similar distribution but only weak to moderate intensity. Original magnification x400.

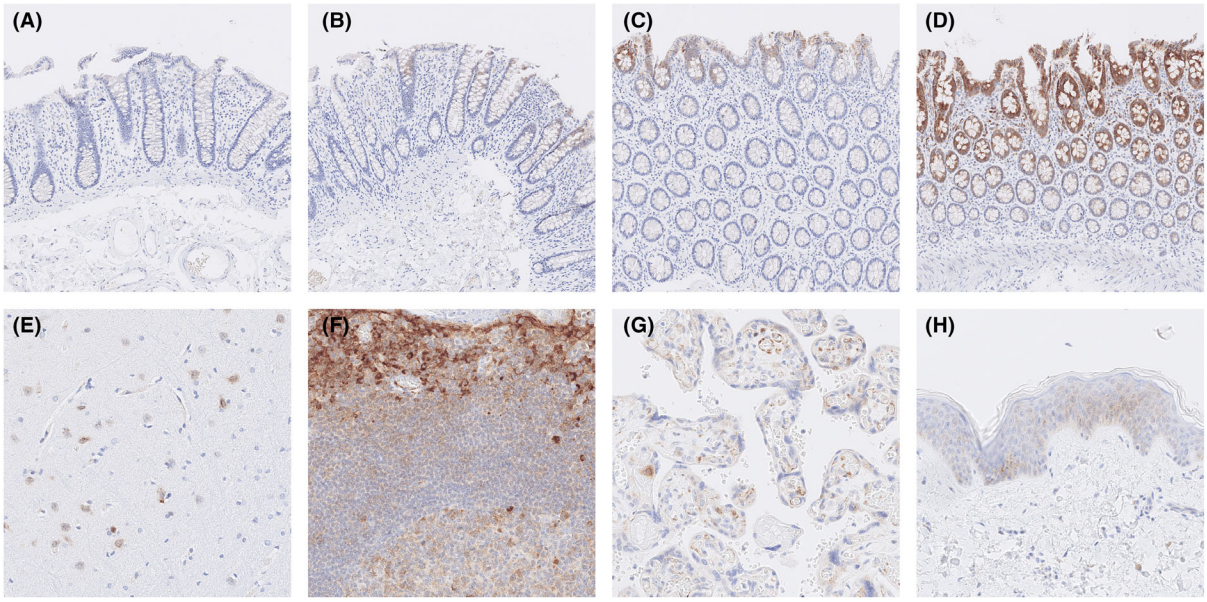

Fig. 2. dsRNA expression (brown) in normal tissue samples by antibody clone 9D5. (A-D), Colon samples from the same patient, fixed in formalin for 3, 24, 48, and 168 h, respectively. Longer formalin fixation time is associated with increased signal intensity. (E) Brain tissue. Weak to moderate reaction in several neurons. (F) Tonsil. Strong reaction in the squamous epithelium (top), moderate reaction in the germinal center (bottom), and weak reaction in lymphocytes (middle). (G) Placenta. Moderate to strong reaction in endothelium and a few stromal cells. (H) Skin. Weak to moderate reaction in the squamous epithelium.

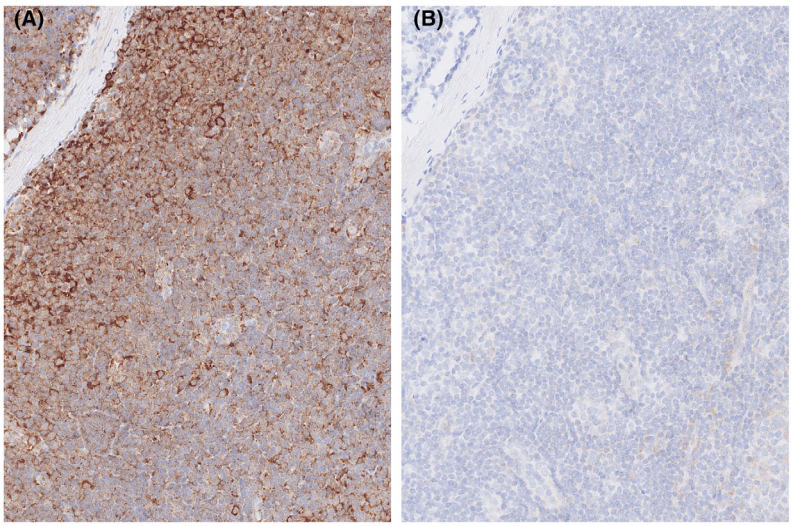

Fig. 3. Effect of RNAse-III pretreatment on dsRNA positivity. (A) Strong positive reaction for dsRNA in tonsillar tissue. (B) Pretreatment by RNAse-III results in a marked reduction or total abrogation of the dsRNA signals. Original magnification x200.

feeble reaction in the tissues with 3 h fixation. By contrast, the signal intensity increased with a longer fixation time (24–168 h). Regarding the tonsils, signals first appeared in the squamous epithelium and subsequently in the lymphoid tissue. In the colorectal mucosa, signals started most luminal and extended more basally with increasing fixation time (see Fig. 2). This tendency was seen for both antibody clones, 9D5 and J2, but the reactions were more intense with 9D5.

DISCUSSION

Our results show to the best of our knowledge, for the first time, that the antibody clone 9D5 directed against dsRNA can be used in FFPE tissue. The staining achieved with the antibody 9D5 had a similar pattern to the more established antibody J2. However, it displayed a better signal-to-noise ratio and generally stronger signals, which is consistent with earlier findings in cell cultures [6]. Also, in accordance with previous reports, we observed a marked reduction in signal intensity after treatment with RNAse III, which specifically degrades dsRNA, supporting a specific IHC reaction with dsRNA [6,11]. Nevertheless, the intensity of the staining reaction was affected by fixation with higher intensity following a longer fixation time and, in some cases, the anti-dsRNA IHC reaction may not be representative for replicative virus.

A strength of this study was the inclusion of a higher number of infected tissues with more different viruses compared to previous studies of dsRNA in FFPE tissues. Additionally, many normal tissues have been investigated. We used clinical material, which is advantageous because the findings can be generalized to clinical settings. However, the material is not as standardized as in experimentally controlled conditions and can be more challenging to interpret. A study limitation was the restricted number of available RNA-virus-infected tissues. We had only one virus with a +ssRNA genome (SARS-CoV2) – all others were DNA viruses. Richardson *et al*. have previously demonstrated dsRNA in infected FFPE tissues with viruses containing positive-sense ssRNA, dsRNA, and dsDNA genomes [11]. So far, dsRNA has not been investigated in FFPE tissue infected with negative-sense ssRNA viruses.

A varying correlation between the virus-specific markers and the presence of dsRNA was observed in the virus-infected tissues. In accordance with earlier reports by others, we observed a similar number and distribution of SARS-CoV-2 virus protein- and dsRNA-positive cells [1]. HSV IHC revealed a higher number of infected cells than dsRNA positive. Previous studies of HSV-infected cell cultures showed a positive reaction for dsRNA with the clone J2 [14], but to our knowledge, dsRNA has not been described in histological samples with HSV. The observed discrepancy between infected and dsRNA-positive cells may at least partly be explained by HSV-encoded proteins that antagonize the production of dsRNA [17]. An opposite trend was seen for the CMV- and HPV-infected tissues with more dsRNA-positive cells than virus protein-containing cells. The antibody cocktail used for CMV detection targets two 'early' proteins that may be expressed only during a distinct phase of infection. The HPV IHC was positive in the most superficial layers of the squamous epithelium, while dsRNA was positive in the basal and spinous layers. Likewise, that might reflect different stages of viral replication and virus assembly. All EBV-infected cases were judged as being dsRNA-negative. The expression in the normal-sized lymphoid cells matched the corresponding uninfected tissues, while the large, EBER-positive cells showed no or only low-staining reaction. As with HSV, this may be due to EBV-encoded dsRNA-antagonizing proteins [18].

Surprisingly, many histologically normal tissue samples exhibited positivity for dsRNA. The reaction was distinct and restricted to specific cell types. Positive normal cells have not been described in the few earlier studies of dsRNA in FFPE tissue [1,11,19]. The origin of the dsRNA staining reaction in normal tissues remains uncertain. At least three possible explanations exist:

1. It represents an unrecognized viral infection (exogenous dsRNA). For example, many excised hyperplastic tonsils may harbor unrecognized viral infections [20].
2. It represents endogenous dsRNA. That has been described in cell cultures but not in FFPE tissues [12]. Endogenous dsRNA would be expected mainly in the nucleus and mitochondria [10]. In most tissues, we observed sparse signals in the nuclei and a more intense and widespread reaction in the cytoplasm. However, the distribution between the nucleus and cytoplasm in the brain tissues tended to be more toward the nuclei. Light microscopy could not determine whether the cytoplasmic staining reaction was within or outside mitochondria.
3. It represents artificial RNA structures formed during formalin fixation that anti-dsRNA antibodies can detect. Previous studies have indicated that formalin cross binds RNA strands [21], but whether it creates binding sites for anti-dsRNA antibodies remains unknown. Mateer *et al*. [22] reported background staining reaction with 9D5 when they used formalin as a fixative but not when they used methanol. That finding supports a potentially artificial formation of dsRNA during formalin fixation and would explain the observed correlation between fixation time and signal intensity.

The observation of dsRNA staining reaction in morphologically normal FFPE tissues underlines the importance of control tissue of the same type and with a comparable fixation to the tissue

under investigation. We have applied the anti-dsRNA assays on additional normal tissues (data not presented) and observed positive reactions in various cell types, including thyroid follicular and pancreatic acinar cells. Positivity was also seen in the basal layers of the urothelium and non-keratinized squamous epithelium. All these cell types represent cells with high secretory or proliferative activity. We speculate that this is due to large amounts of mRNA – susceptible to cross binding by formalin – in these cell types. That would support the third of the abovementioned explanations.

Given that the observed staining reactions represent biologically genuine dsRNA, the IHC assay based on Ab clone 9D5 enables researchers to investigate the possible relationship between dsRNA and various diseases. That applies to both viral infections and the possible role of endogenous dsRNA in developing inflammatory and degenerative disorders, as well as cancer [23]. If the opposite is true and the dsRNA in uninfected cells is a consequence of formalin fixation, one must be careful when interpreting the results.

In conclusion, this study introduces the monoclonal anti-dsRNA Ab 9D5 as a potential IHC marker for dsRNA in FFPE tissue, providing a better signal-to-noise ratio than the established Ab clone J2. dsRNA was demonstrated in most cases of viral infection, but despite a high analytical specificity, the clinical specificity was low. Therefore, one must be very cautious in the interpretation of the results. The sole detection of dsRNA does not allow firm conclusions regarding the presence of viral infections. However, it may serve well as a first-line screening marker, but with a need for other markers to confirm positive results.

The authors want to thank Mia Korsdal Stensballe for her excellent help with performing the immunohistochemistry and the production of TMAs.

DISCLOSURE

No external funding has been received.

REFERENCES

1. Lean FZX, Lamers MM, Smith SP, Shipley R, Schipper D, Temperton N, et al. Development of immunohistochemistry and in situ hybridisation for the detection of SARS-CoV and SARS-CoV-2 in formalin-fixed paraffin-embedded specimens. Sci Rep. 2020;10:21894.
2. Nyström N, Berg T, Lundin E, Skog O, Hansson I, Frisk G, et al. Human enterovirus species B in ileocecal Crohn's disease. Clin Transl Gastroenterol. 2013;4:e38.
3. Rodriguez-Calvo T. Enterovirus infection and type 1 diabetes: unraveling the crime scene. Clin Exp Immunol. 2019;195:15–24.
4. Shieh W-J, Zaki SR. Advanced pathology techniques for detecting emerging infectious disease pathogens. In: Tang YW, Stratton CW, editors. Advanced techniques in diagnostic microbiology. Boston, MA: Springer; 2013. p. 873–90.
5. Sanjuán R, Domingo-Calap P. Mechanisms of viral mutation. Cell Mol Life Sci. 2016;73:4433–48.
6. Son K-N, Liang Z, Lipton HL. Double-stranded RNA is detected by immunofluorescence analysis in RNA and DNA virus infections, including those by negative-stranded RNA viruses. J Virol. 2015;89:9383–92.
7. Schneider WM, Chevillotte MD, Rice CM. Interferon-stimulated genes: a complex web of host defenses. Annu Rev Immunol. 2014;32:513–45.
8. Onoguchi K, Yoneyama M, Fujita T. Retinoic acid-inducible gene-I-like receptors. J Interferon Cytokine Res. 2011;31:27–31.
9. Pindel A, Sadler A. The role of protein kinase R in the interferon response. J Interferon Cytokine Res. 2011;31:59–70.
10. Sadeq S, Al-Hashimi S, Cusack CM, Werner A. Endogenous double-stranded RNA. Non-coding RNA. 2021;7(1):1–18.
11. Richardson SJ, Willcox A, Hilton DA, Tauriainen S, Hyoty H, Bone AJ, et al. Use of antisera directed against dsRNA to detect viral infections in formalin-fixed paraffin-embedded tissue. J Clin Virol. 2010;49:180–5.
12. Dhir A, Dhir S, Borowski LS, Jimenez L, Teitell M, Rötig A, et al. Mitochondrial double-stranded RNA triggers antiviral signalling in humans. Nature. 2018;560:238–42.
13. Bonin M, Oberstraß J, Lukacs N, Ewert K, Oesterschulze E, Kassing R, et al. Determination of preferential binding sites for anti-dsRNA antibodies on double-stranded RNA by scanning force microscopy. RNA. 2000;6:563–70.
14. Weber F, Wagner V, Rasmussen SB, Hartmann R, Paludan SR. Double-stranded RNA is produced by positive-Strand RNA viruses and DNA viruses but not in detectable amounts by negative-Strand RNA viruses. J Virol. 2006;80:5059–64.
15. Schonborn J, Oberstraß J, Breyel E, Tittgen J, Schumacher J, Lukacs N. Monoclonal antibodies to double-stranded RNA as probes of RNA structure in crude nucleic acid extracts. Nucleic Acids Res. 1991;19:2993–3000.
16. Mateer EJ, Paessler S, Huang C. Visualization of double-stranded RNA colocalizing with pattern recognition receptors in arenavirus infected cells. Front Cell Infect Microbiol. 2018;8:1–9.
17. Dauber B, Saffran HA, Smiley JR. The herpes simplex virus host shutoff (vhs) RNase limits accumulation of double stranded RNA in infected cells: evidence for accelerated decay of duplex RNA. PLoS Pathog. 2019;15(10):e1008111.

18. Poppers J, Mulvey M, Perez C, Khoo D, Mohr I. Identification of a lytic-cycle Epstein-Barr virus gene product that can regulate PKR activation. J Virol. 2003;77:228–36.
19. Debes JD, Groothuismink ZMA, Doukas M, de Man RA, Boonstra A. Immune dissociation during acute hepatitis E infection. Int J Infect Dis. 2019;87:39–42.
20. Silvoniemi A, Mikola E, Ivaska L, Jeskanen M, Löyttyniemi E, Puhakka T, et al. Intratonsillar detection of 27 distinct viruses: a cross - sectional study. J Med Virol. 2020;92:3830–8.
21. Evers DL, Fowler CB, Cunningham BR, Mason JT, O'leary TJ. The effect of formaldehyde fixation on RNA optimization of formaldehyde adduct removal. JMDI. 2011;13:282–8.
22. Mateer E, Paessler S, Huang C. Confocal imaging of double-stranded RNA and pattern recognition receptors in negative-sense RNA virus infection. J Vis Exp. 2019;(143):e59095. https://doi.org/10.3791/59095
23. Kim S, Ku Y, Ku J, Kim Y. Evidence of aberrant immune response by endogenous double-stranded RNAs: attack from within. Bioessays. 2019;41:1–12.